Journal Name

ARTICLE

Probing the degradation and homogeneity of embedded perovskite semiconducting layers in photovoltaic devices by Raman spectroscopy†

Received 00th January 20xx,
Accepted 00th January 20xx

DOI: 10.1039/x0xx00000x

www.rsc.org/

K. E.A. Hooper,[a] H. K.H. Lee,[a] M. J. Newman,[a] S. Meroni,[a] J. Baker, [a] T. M. Watson[a] and W. C. Tsoi*[a]

The key challenges for perovskite solar cells include their poor stability and film homogenity. Studying the degradation and homogenity of perovskite layers within device structures can be challenging but critical to the understanding of stability and effect of processing in real life conditions. We show that Raman spectroscopy (RS) is a unique and powerful method (simple and fast) to probe the degradation of the perovskite film within the device structure and image perovskite formation. We demonstrate that RS can be used to directly probe chemical (PbI_2) and physical (dihydrated phase) degradation of a perovskite film, and estimate the relative amount of the degradation species formed, mapping its distribution with ~1µm spatial resolution. This has been applied to mapping a large area perovskite module to characterise the effacy of PbI_2 to perovskite conversion. We also use RS to study the degradation species and kinetics under diverse accelerated degradation conditions (temperature and humidity) in-situ. These capabilities are difficult to achieve with other methods, presenting RS as an important tool to gain understanding of the degradation and effect of processing on perovskite-based photovoltaic devices.

Introduction

The interest in lead halide perovskite materials for photovoltaic (PV) application has increased dramatically since their initial use in 2009,[1] with breakthrough developments in device architecture in 2012[2] and efficiencies now >20 %.[3,4] Their high performance and potential for low cost manufacture[5,6] present them as a very attractive candidate to rival other PV technologies. Two of the main bottlenecks to the commercialization of perovskite solar cells (PSCs) are device stability and homogeneity of the perovskite films. Perovskite materials can be degraded by light, oxygen, temperature, and humidity.[7-10] In order to improve the stability of perovskite materials it is crucial to understand the degradation mechanisms. Although there are many degradation studies on PSCs, most of the studies are based on measuring the device efficiencies, or characterization of bare perovskite films. However, it is critical to probe the stability of the perovskite film within a complete device since their stability is likely to be significantly influenced by the multiple layers and interfaces. The ability to selectively probe the perovskite layer within a device is important to identify the degradation source and distinguish it from the influence of other layers in the device. Methods to image the chemical distribution of perovskite PV materials in the device are also important to study the homogeneity of the films, this is particularly important for large area perovskite PV modules.

Raman spectroscopy (RS) is a powerful vibrational spectroscopic technique which can be used to directly probe chemical and physical interactions (the vibrational modes obtained act as fingerprints of the materials) in a very simple and fast way. It has been applied to study degradation, crystallization and interfacial interaction of organic solar materials.[11-13] Recently RS has been applied to study the chemical structures of bare perovskite PV films,[14-16] but remains largely unexplored in full devices. One of the challenges is that the Raman signals from perovskite films are weak and can be noisy. The signal can be improved by increasing the intensity of the excitation laser, but the films are susceptible to degradation by the laser (particularly those that emit visible light). Here, we found that the top layers (spiro-OMeTAD or spiro-OMeTAD/Au) of the device provide significant protection to the underlying perovskite film from degradation by the laser (532 nm). Additionally the Raman signals from the degradation products (e.g. PbI_2) are much stronger than those of non-degraded perovskite film. This allows us to probe for the first time the degradation of the perovskite film embedded within the device structure. We also demonstrate large area Raman mapping (in cm scale; note Raman mapping usually performed in µm scale) for the first time. The mapping technique is used to investigate the

[a] SPECIFIC, College of Engineering, Swansea University, Bay Campus, Fabian Way, Swansea, SA1 8EN, UK
*Email: W.C.Tsoi@Swansea.ac.uk
†Electronic Supplementary Information (ESI) available: See DOI: 10.1039/x0xx00000x

homogeneity of the perovskite film in a large area perovskite module. These results show that RS can be a unique and powerful method to characterize chemical/physical degradation and perovskite formation in full devices, which has been difficult to achieve by other methods.

The main device structure studied is FTO/c-TiO_2/m-TiO_2/MAPI/spiro-OMeTAD/Au (one of the original standard architectures). FTO, c-TiO_2, m-TiO_2, MAPI, spiro-OMeTAD, and Au refer to fluorine doped tin oxide, compact titanium dioxide, meso-porous TiO_2, methyl ammonium lead iodide, 2,2',7,7'-Tetrakis[N,N-di(4-methoxyphenyl)amino]-9,9'-spirobifluorene, and gold, respectively. Films and devices were fabricated based on the sequential deposition method.[17] Individual layers were prepared in an identical fashion to the corresponding layer in a full device. For a perovskite PV module, the structure studied is glass/FTO/c-TiO_2/m-TiO_2/MAPI/m-ZrO_2/m-carbon where m-ZrO_2 and m-carbon are mesoporous. This device structure and processing method has the advantage of being a hole-conductor-free, printable PSC.[18,19]

Results and discussion

Raman measurements of embedded perovskite film

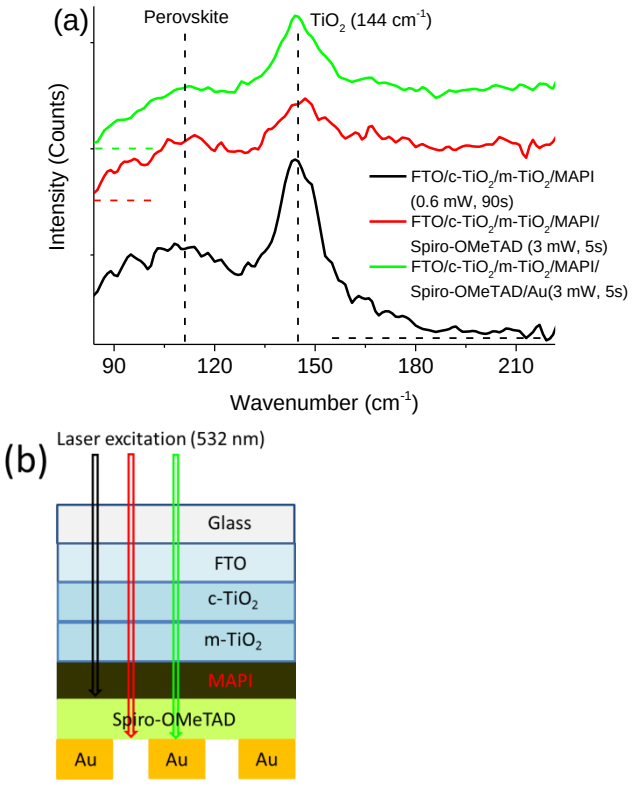

Fig. 1 (a) Raman spectra of embedded perovskite layer (probed through glass side). The spectra are offset and the horizontal dashed lines are the zero levels, (b) schematic figure showing the probing through glass side. The colours of the arrows corresponding to the colours of the spectra in (a). For the spectrum of FTO/c-TiO_2/m-TiO_2/MAPI, spiro-OMeTAD and Au were not deposited on the MAPI layer.

Fig. 1a shows the Raman spectra of the buried perovskite layers within a device stack (device efficiency ~11-12 %: see Table S1 & S2 and Fig. S1 & S2 for details in the ESI†). These measurements were enabled by probing the samples through the glass side of the device as shown in Fig. 1b. Importantly, the Raman spectra of FTO/c-TiO_2/m-TiO_2/MAPI (probed from the glass side) shows a broad peak at ~110 cm^{-1} which has been assigned to librational modes of the methyl ammonia (MA) cations of MAPI.[14,15] This result shows that embedded MAPI layer can be probed by RS. The Raman signals from the perovskite film have some noise which is due to the weak Raman signal from the perovskite. This weak signal can be due to the small Raman scattering cross-section (which determine the magnitude of Raman signal) of the librational modes of the MA cations at the excitation wavelength.[20] It has been proposed that the broad signal of the MA cations librational modes can be assigned to their disorder which arises from additional degrees of rotational and torsional freedom.[14,21] For all figures in this paper, the background levels have not been subtracted, as the subtractions can lead to further error since the signals are weak and the background levels can be non-linear.

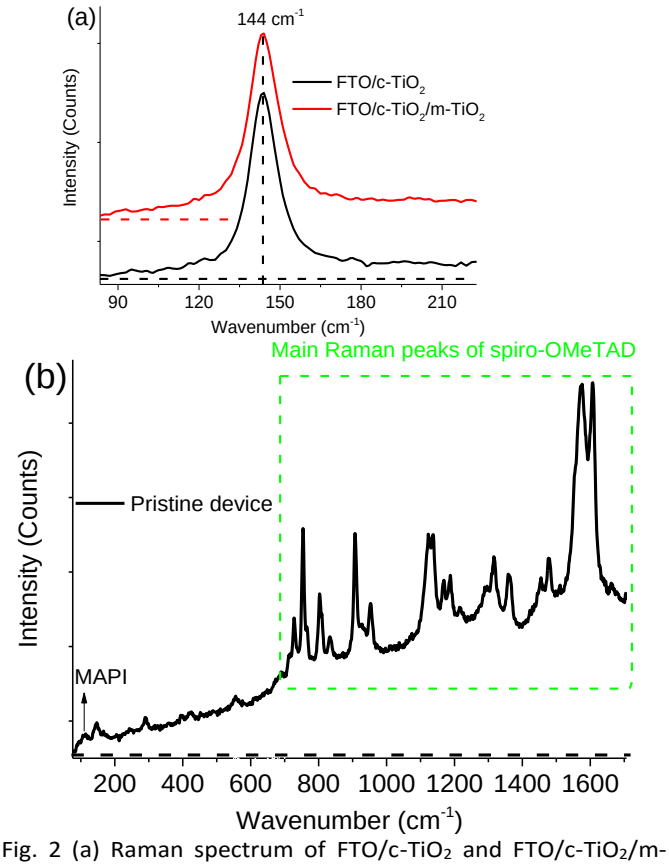

Fig. 2 (a) Raman spectrum of FTO/c-TiO_2 and FTO/c-TiO_2/m-TiO_2 (probing conditions are: 6 mW, 10s, accumulation 3), and (b) Raman spectrum of the pristine a MAPI device. Probing conditions are: 3mW, 5s. The spectra are offset, and the horizontal dashed lines are the zero levels.

The Raman peak at 144 cm^{-1} in Fig. 1a can be assigned to the anatase phase of TiO_2 as shown in Fig. 2a.[22] Critically, the Raman spectrum of FTO/c-TiO_2/m-TiO_2/MAPI/spiro-OMeTAD also shows the Raman signals from MAPI since the Raman signal from spiro-OMeTAD does not overlap with that of the perovskite. This ensures that the Raman signal from the MAPI layer is observable (see Fig. 2b) despite the spiro-OMeTAD signal being significantly stronger. As also shown in Fig. 1a, the ability to characterize perovskite layers within the device (FTO/c-TiO_2/m-TiO_2/MAPI/spiro-OMeTAD/Au) is a powerful tool which is difficult to achieve by most characterization methods.

Effect of bottom and top layers on the degradation of the perovskite film

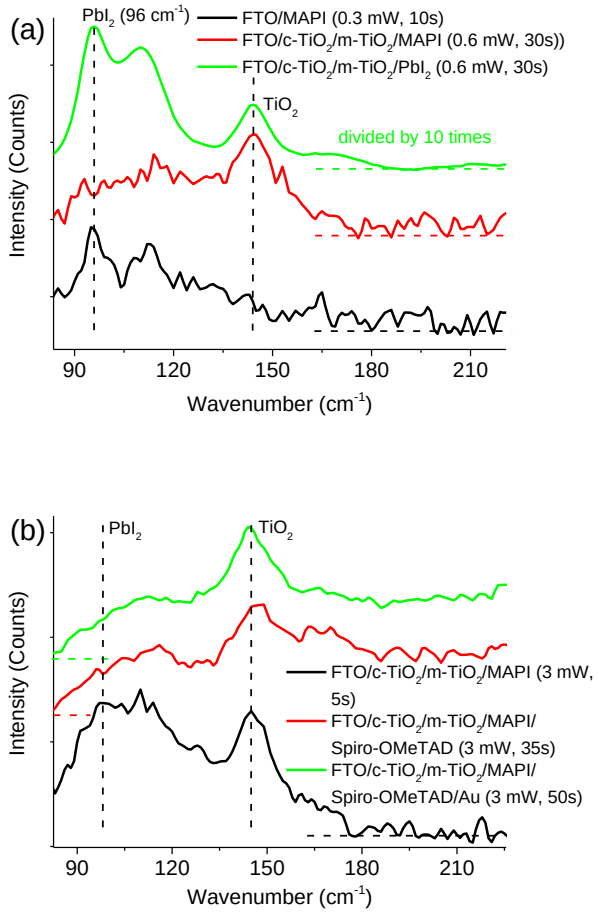

Fig. 3(a) Raman spectra of MAPI films on different substrates and PbI_2 film, and (b) Raman spectra of MAPI film with and without top layers. The spectra are offset and the horizontal dashed lines are the zero levels

Interestingly, the laser used for RS can be used deliberately to accelerate the photo-degradation of the MAPI film by tuning to stronger exposure conditions. Figure 3a shows the Raman spectra of FTO/MAPI, FTO/c-TiO_2/m-TiO_2/MAPI and PbI_2 films. The MAPI deposited on c-TiO_2/m-TiO_2 has considerably less photo-degradation compared with perovskite deposited on FTO despite the fact that the MAPI deposited on c-TiO_2/m-TiO_2 was subjected to a higher probing power for a longer time. This is supported by the lack of PbI_2 signal (peak at ~96 cm^{-1})[15,16] in the FTO/c-TiO_2/m-TiO_2/MAPI film, while a PbI_2 signal was observed in the FTO/MAPI film. This result shows that the substrate that the MAPI film is deposited onto can play an important role in its photo-stability. It has been proposed that photo-excited MAPI reacts with oxygen to form superoxide ($O_2^{\bullet-}$) which causes degradation to form PbI_2:[23]

$$CH_3NH_3PbI_3 + O_2^{\bullet-} \xrightarrow{Deprotonation} CH_3NH_2 + PbI_2 + I/2I_2 + H_2O \quad (1)$$

The result in Figure 3a can be explained by a higher rate of superoxide reduction with m-TiO_2 than FTO, as electron transfer from photoexcited MAPI (a process quench the superoxide formation) to m-TiO_2 is more efficient than to FTO.[23] This is consistent with a better matching of the electronic energy level of m-TiO_2 (conduction band (CB) ~-4.1 eV) with MAPI (CB ~-3.9 eV) compared with that of FTO (work function~-4.4 eV).

Note that the Raman signal from a PbI_2 film observed is ~ 20 times larger than that of MAPI film (see Fig. 3a the signal from PbI_2 is ~2 times higher than from MAPI after divided the PbI_2 spectrum by 10). The stronger signal from PbI_2 shows that RS is more suitable to probe the degradation product (or the precursor when PbI_2 acts as precursor) compared with MAPI which has weak Raman signal. Fig. 3b shows the Raman spectra of the MAPI in a device stack with and without top layers. In the structure of FTO/m-TiO_2/c-TiO_2/MAPI, the MAPI was degraded by the laser using a probing power of 3mW and a probing time of 5s (with Raman peaks at similar position to PbI_2 and stronger Raman signal like PbI_2). Importantly, when spiro-OMeTAD and Au were deposited on top of MAPI film, no peaks related to PbI_2 formation were observed even with ≥ 7 consecutive measurements (Fig. 3b). These results show that the layers on top of MAPI film can significantly protect the MAPI film from the laser's accelerated photo-degradation. The Raman signals contain more noise in Fig. 3a than Fig. 1a, as weaker excitation conditions were used.

Microscopic distribution of degradation product of buried MAPI in degraded devices

For a deeper insight into the distribution of MAPI degradation within a PSC, devices were annealed at 150°C for 2 hours to accelerate thermal degradation. Optical imaging, Raman mapping of PbI_2 (at 96 cm^{-1}) and photoluminescence (PL) mapping of MAPI (at 770 nm)[16] were performed on the same region inside the device pixel with a spatial resolution of ~ 1µm.

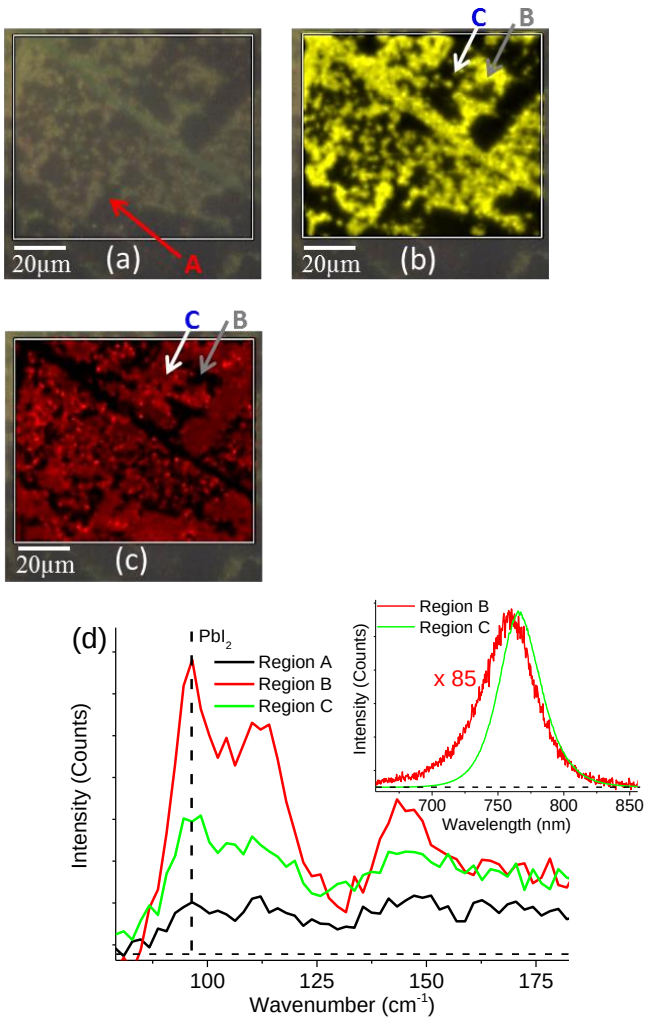

Fig. 4 (a) Optical image, (b) Raman map of PbI_2 (96 cm^{-1}), (c) PL map of MAPI (770 nm) of a device thermally degraded, and (d) Raman spectra at the labelled regions. Inset shows the PL spectra at the labelled regions. The horizontal dashed lines are the zero levels.

The optical image (Fig. 4a) shows yellow and brown regions which are likely to be PbI_2 (degradation product) and less degraded MAPI,[24] respectively. Importantly, it shows that under the same degraded temperature, even regions physically close to each other (in µm scale) can degrade differently. The Raman mapping of PbI_2 (Fig. 4b) directly correlates with the yellow regions, supporting that the yellow region contains PbI_2. The inhomogeneous degradation is likely to be related to the inhomogeneity of the MAPI film formed.[25] This result could imply that the layer underneath the perovskite layer, which impacts the deposition of the perovskite layer, influences the rate/extent of degradation. In some areas where the optical image does not appear yellow (see region A in Fig.4a), RS is able to probe some PbI_2 signals (see region A in Fig. 4d) giving insight which is not possible with the optical image alone.

Figure 4b & c show that as the MAPI is degraded to PbI_2, the PL signal (770 nm) from MAPI is reduced dramatically (comparing region C with B). Fig. 4d shows the Raman spectra at region B and C (Fig. 4b). Interestingly, although the Raman signal at region B (more PbI_2) is only ~2 times higher than that of region C (Fig. 4d), the PL signal at region B is ~85 weaker (also blue shifted) than that of region C (inset of Fig. 4d). As PbI_2 does not absorb considerably at 532nm (the excitation wavelength), i.e. under non-resonant Raman condition, the PbI_2 signal can be estimated to be proportional to the amount of PbI_2 formed. It is likely that PL is sensitive to more complicated photo-physical/-chemical process which does not directly correlate to the amount of PbI_2 formed. It is very important to note that comparing with the optical image and PL, RS is unique in terms of directly probing chemical species. This capability allows the estimation of the relative amount of PbI_2 formed, therefore tackling an important challenge where other techniques may struggle. Furthermore, the Raman mapping on ambient aged $CH_3NH_3PbI_{3-x}Cl_x$ device with planar structure also show a PbI_2 degradation product with inhomogeneous spatial distribution (see Fig. S3 in the ESI†). These results show that RS is powerful to study a range of different perovskite materials, device structures, and degradation conditions.

In-situ Raman measurements of the degradation of the embedded perovskite layer under accelerated conditions

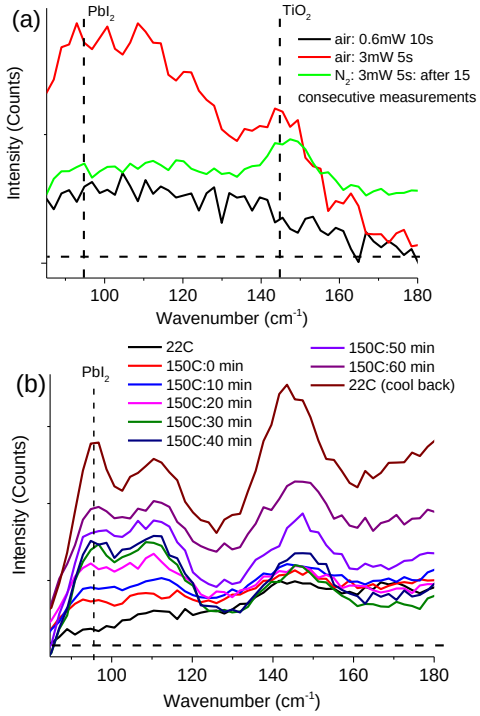

Fig. 5 (a) Raman spectra of MAPI/m-TiO_2/c-TiO_2/FTO in ambient air and in nitrogen (probe through MAPI), and (b) In-situ Raman spectra of the device versus temperature and time (probed through spiro-OMeTAD). The horizontal dashed lines are the zero levels.

To gain more insight into the degradation kinetics of the MAPI layer, in-situ RS measurements with light (in ambient air and nitrogen), temperature and humidity were performed. As shown in Fig. 5a, the MAPI degraded to form PbI_2 in ambient air (also supported by the enhanced signal at the PbI_2 spectral region) while there is no PbI_2 signal observed in a nitrogen environment even after 15 consecutive measurements. This result is consistent and supports Eq. (1) that the superoxide formation is suppressed without oxygen. The enhanced photo-stability of MAPI with spiro-OMeTAD and Au top layers is consistent with the layers protecting the MAPI being directly exposed to oxygen to form superoxide. The MAPI under the Au/spiro-OMeTAD still appears brown after illumination at 85 mW/cm^2 for 8 hours (through glass side and in air) using a solar simulator, while the MAPI covered only by spiro-OMeTAD region appeared yellow in colour. This result is consistent with increased protection to oxygen exposure of the MAPI by the extra (Au) top layer.

Fig. 5b shows the in-situ temperature (and time) dependent RS measurement in ambient air on the MAPI (probing through the spiro-OMeTAD region of the device). The device was heated to 150°C to accelerate the thermal degradation (same temperature as used by Stranks et al.[24]) The embedded MAPI film degraded to form PbI_2 in less than 10 mins, which is consistent with the following chemical equation:[26]

$$CH_3NH_3PbI_3 \rightarrow PbI_2 + CH_3NH_2\uparrow + HI\uparrow \quad (2)$$

The PbI_2 Raman signal remains after the device was cooled back to 22°C, showing it is a non-reversible degradation process. The PbI_2 Raman signal at the Au/spiro-OMeTAD region is similar to that of the spiro-OMeTAD region (shown in Fig. 5b) after being cooled back to 22°C, unlike the photo-degradation. This difference suggests that the thermal degradation is a bulk effect for the whole MAPI film and is more determined by the homogeneity of the perovskite film formed and therefore the top layers are not that critical. This result is consistent with ex-situ thermal degradation (annealed at 150°C for 2 hours in air) of the device, which shows that the MAPI film was degraded to similar yellow colour at both the MAPI/spiro-OMeTAD and MAPI/spiro-OMeTAD/Au regions (these two regions are shown in Fig. 1b).

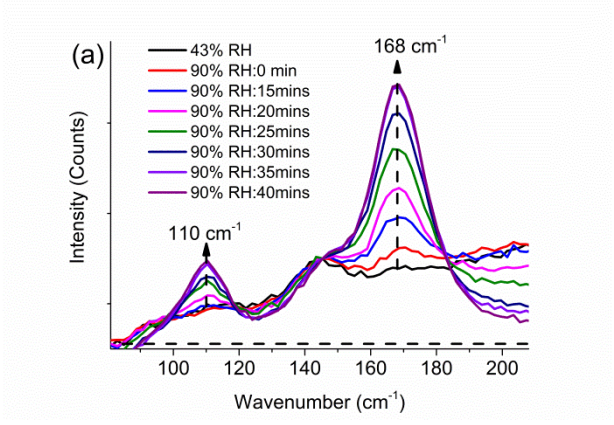

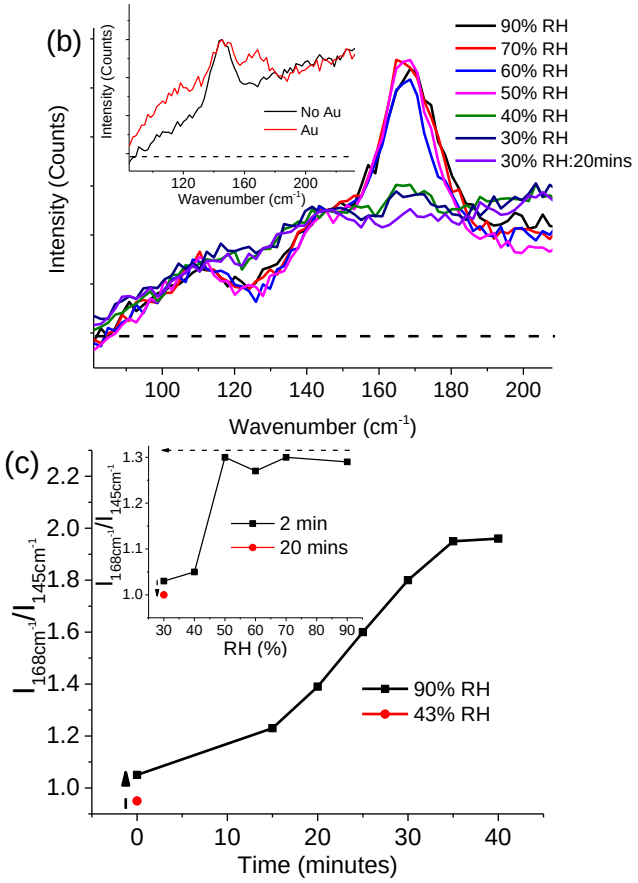

Fig. 6 In-situ Raman spectra of the device (probed through spiro-OMeTAD): (a) with increased humidity and time, and (b) with decreased humidity (inset shows Raman spectra at the spiro-OMeTAD, and spiro-OMeTAD/Au regions after dried, respectively). The horizontal dashed lines are the zero levels. (c) $I_{168cm^{-1}}/I_{145cm^{-1}}$ with increased humidity and time. Inset shows $I_{168cm^{-1}}/I_{145cm^{-1}}$ versus decreased humidity. All measurements were performed in the dark.

As humidity is generally believed to be critical to the degradation of perovskite films, in-situ humidity (and time) dependent RS of the MAPI layer (probed through the spiro-OMeTAD region) within the device was studied. For accelerated studies in the dark, the humidity was raised to 90.0 ± 0.5 % RH. As shown in Fig. 6a, after less than 10 mins at 90.0 %RH, peaks at 168 cm^{-1} and 110 cm^{-1} appear, and these peaks grow until 35 mins when they saturate (during this time the device turned pale yellow). It has been proposed that MAPI can interact with moisture in the following way:[7,27]

$$4(CH_3NH_3)PbI_3+4H_2O \rightleftharpoons (CH_3NH_3)_4PbI_6\bullet 2H_2O+3PbI_2+2H_2O \quad (3)$$

It is also proposed that upon exposure to humid air in dark, dihydrated perovskite $(CH_3NH_3)_4PbI_6$ can be formed without formation of PbI_2.[28] Our results match well with the formation of dihydrated MAPI without forming PbI_2, since we did not observe a Raman signal attributable to PbI_2 at 96 cm^{-1}. For more quantitative study, the intensity at the 168 cm^{-1} versus that at the 145 cm^{-1} (the signal from TiO_2) ($I_{168cm^{-1}}/I_{145cm^{-1}}$) in Fig. 6a is plotted in Fig. 6c. As shown in Fig. 6c, at 90% RH,

$I_{168cm^{-1}}/I_{145cm^{-1}}$ increases at a rate of ~0.012/min in the first 15 mins ($I_{168cm^{-1}}/I_{145cm^{-1}}$ ~0.95 at 43% RH), and then increases at a faster rate (0.036/min) up to 35 mins. After 35 mins, $I_{168cm^{-1}}/I_{145cm^{-1}}$ tends to saturate (~1.96).

As shown in Fig. 6b and inset in Fig. 6c, $I_{168cm^{-1}}/I_{145cm^{-1}}$ remains at a similar magnitude~ 1.29 when the device is dried from 90% RH to 50% RH (held ~ 2 minutes at each RH). However the ratio $I_{168cm^{-1}}/I_{145cm^{-1}}$ drops significantly at ≤ 40% RH (~1.04), and continues to drop with 20 mins drying time, becoming similar to the spectrum before the humidity was raised (~1.00). The colour of the device also changes back to brown (although paler). These results are consistent with, and support the reversible (at least semi-reversible) dihydration process of the MAPI. Note that the lower $I_{168cm^{-1}}/I_{145cm^{-1}}$ value at 90% RH (~ 1.29) compared with that in Fig. 6c (~1.96) is mainly due to shorter exposure time to high humidity (2 mins at 90% RH versus 40 mins in Fig. 6c).

Importantly, the two Raman peaks were still observable in the spiro-OMeTAD/Au region (but not at the spiro-OMeTAD region) with the drying timescale used (~30 mins, see inset of Fig. 6b). This result suggests that dihydrated perovskite species still remain at the Au region (consistent with higher degree of moisture trapping at this region). This could be relevant to device degradation. These findings may have important implications that the device performance could be recovered significantly if the trapped moisture can be dried out (e.g. over longer times). This result supports the findings by Leguy et al. which shows the efficiency of MAPI device is nearly fully recovered after sufficient drying.[27]

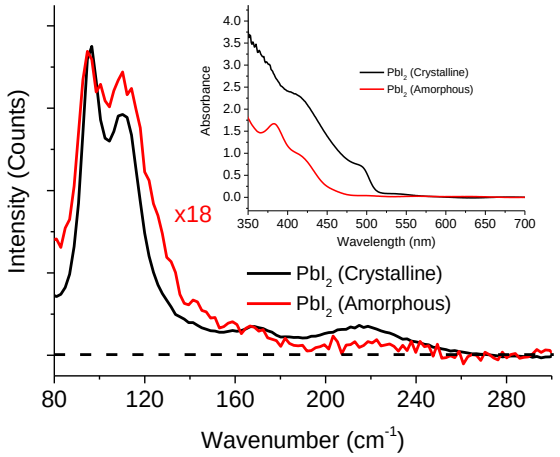

Fig. 7 Raman spectra of crystalline and amorphous PbI_2 films on FTO. Probing conditions are: 0.6 mW, 30s. Thicknesses of the films are ~ 120 nm. The horizontal dashed line is the zero level. Inset shows their absorbance spectra.

To understand the origins of the peaks, and identify any possible amorphous PbI_2 formation (which has previously been suggested to form during the process of dihydration[27]), neat amorphous PbI_2 films were prepared following the procedures used in ref. 29. Fig. 7 shows that the Raman spectrum of amorphous PbI_2 is similar to crystallized PbI_2 (also peak at 96 cm^{-1}) but with ~18 times less signal. The weaker Raman signal can be correlated to weaker absorption of the amorphous phase at the laser excitation (532 nm) (see inset of Fig. 7). The absorbance spectrum is same as that in ref. 29 showing the formation of amorphous phase. Therefore, we assign the rising peaks at 168 cm^{-1} and 110 cm^{-1} to the formation of the dihydrated MAPI (enhanced signal at 110 cm^{-1} is consistent with enhanced librational modes of the MA cations). The Raman signal from amorphous PbI_2 is comparable to MAPI under similar probing conditions. As the Raman signal from amorphous PbI_2 is not observed when MAPI is dihydrated, there is no evidence that PbI_2 was formed. Importantly RS can also be used to probe amorphous PbI_2 which can be problematic using conventional X-ray diffraction technique. It is likely that whether PbI_2 will be formed during the process of dihydration is also determined by other environmental factors (e.g. air/nitrogen, dark/light, during the exposure to the high humidity levels). Measurements in ref. 27 were performed in humid nitrogen, while in ref. 28 were performed in humid air (did not observe PbI_2).

Raman mapping of a large area perovskite PV module

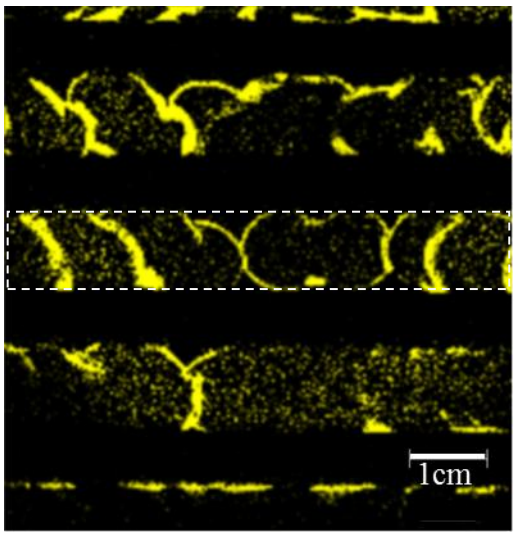

Fig. 8 Raman mapping (PbI_2) of a large area perovskite PV module (glass/FTO/c-TiO_2/m-TiO_2/MAPI/m-ZrO_2/m-carbon). The white broken line highlights one of the active areas.

Figure 8 shows the PbI_2 Raman mapping of a large area perovskite PV module (glass/FTO/c-TiO_2/m-TiO_2/MAPI/m-ZrO_2/m-carbon). The mapping area is ~6.8 cm x 6.5 cm with spatial resolution of ~ 330 µm and mapping time of 75 mins. Drops of PbI_2 were drop cast through the m-carbon/m-ZrO_2 to the patterned FTO region, and the whole sample was dipped in a solution of MAI in IPA to form MAPI (see the experimental section for more details). It shows that in some regions, there remains a significant amount of PbI_2 which does not react with MAI to form MAPI. The relative large arc-shaped features

could be due to the so-called coffee-stain effect,[30] where the PbI_2 at the outside of the ring is more dense and as a result the MAI cannot convert these regions completely. This is the first demonstration of applying Raman mapping to study a perovskite module and across a large area. The strip-shaped features in the mapping are single cells. This result shows that Raman mapping can be very useful to study the processing (and its optimization) of perovskite PV films on large area substrates. This is particularly important for scaling up processing methods (in this study the other layers were deposited by screen printing). The non-optimized device efficiency is consistent with significant regions of PbI_2 which has not converted to MAPI.

The ability to probe the embedded perovskite layer and its degradation quickly within a device stack is very useful to select the appropriate bottom and top layers in terms of photo-stability. Probing the distribution of the degradation species (PbI_2) and quantifying it can be used to probe the homogeneity of the perovskite film formed or to choose the appropriate underneath layer (which the perovskite film will be deposited on homogenously). The in-situ Raman measurements under accelerated degradation conditions should be useful to screen the stability of a particular perovskite layer quickly. The large area Raman mapping can also be applied to study the degradation of perovskite PV modules. It is also important to note that RS is a very simple technique which does not require special sample/device preparation (like our case), unlike e.g. transmission electron microscopy (TEM). The Raman spectra can be obtained with very short acquisition time (usually ≤ 1 min, depending on excitation power without the photo-degradation, it can be ≤ 1s). This capability allows fast in-situ characterization, such as for the accelerated degradation studies here. Moreover RS can also probe the other layers (e.g. spiro-OMeTAD) in the device simultaneously, therefore could provide unique information on the relative contribution of each layer to the device degradation.

Conclusions

We demonstrate for the first time that RS is a unique and powerful technique to tackle the challenge of probing degradation and homogeneity of perovskite PV films within a device stack. We find that the photo-degradation of the perovskite layer is highly determined by both the top and bottom layers. We also show that the relative amount of degradation product (PbI_2) can be estimated, and its distribution can be measured with ~1 μm spatial resolution. Furthermore, we demonstrate that in-situ RS is very useful to study the kinetics of accelerated degradation. The embedded perovskite layer can be thermally degraded and dihydrated in ≤ 10 mins. Both the top and bottom layers can reduce photo-degradation. However the gold layer has no considerable effect to the thermal-degradation, but can trap moisture preventing the reversible dehydration of the dihydrated perovskite phase. We also demonstrate for the first time Raman mapping can be applied to study incomplete conversion of PbI_2 to perovskite in large area perovskite PV modules. We envision that more detailed studies on degradation and homogeneity of perovskite layer within devices will be uncovered by RS. More generally, we also envision that RS will be very useful to study other perovskite semiconductor-based devices.

Experimental section

Preparation of the devices and power conversion efficiency measurements

7 Ω/□ FTO glass (NSG Pilkington) was used as a substrate. A 50 nm thick compact layer of TiO_2 (c-TiO_2) was deposited via spray pyrolysis of titanium diisopropoxide bis(acetylacetonate) in isoproponal at 300°C followed by a 30 min sinter at 550°C. A layer of mesoporous TiO_2 (m-TiO_2) was deposited by spin coating a diluted solution of DSL 18NR-T TiO_2 paste (Dyesol) in ethanol and sintering at 550°C for 30 min (thickness ~200-250 nm). Subsequent layers were prepared under nitrogen in a glove box. Lead iodide films were spin coated from a 1 M solution of PbI_2 in *N,N*-dimethylformamide (DMF) and dried at 70°C for 10 min. PbI_2 films were submerged in a 0.063 M solution of methylammonium iodide (MAI) in isoproponal for 5 min to convert to perovskite - methylammonium lead iodide (MAPI) (thickness ~300 nm). Afterwards they were very briefly rinsed in isoproponal to remove excess MAI then heated at 70°C for a further 30 min. A solution of 2,2′,7,7′-tetrakis(N,N-di-p-methoxyphenyl-amine) 9,9′- spirobifluorene (spiro-OMeTAD) at 75 mg/1 ml of chlorobenzene (also containing 30 μl/ml of tBP and 20 μl/ml of 1.81 M Li-TFSI in acetonitrile) was spin coated onto the perovskite and left in a box of desiccated air for 10 hours to oxygen dope (thickness ~250 nm) before evaporating on gold contacts (thickness ~30 nm).

Masked devices (0.09 cm^2) were tested under a class AAA solar simulator (Newport Oriel Sol3A 94023A) at 1 sun calibrated against a KG5 reference cell (Newport Oriel 91150-KG5).

Raman and PL measurements

The Raman measurements were performed with a Renishaw Invia Raman system in backscattering configuration. The laser excitation is 532 nm, and a 50x long objective was used (NA: 0.50, spot size ~1μm). Raman and photoluminescence (PL) maps were obtained by first obtained a Raman/PL spectrum from a region, then obtained the spectra from the next region using a X-Y scanning stage. Maps can be generated by collecting the spectra from all the scanning regions e.g. by mapping the intensity at a particular spectral region, as used here. In-situ Raman measurements were performed with an environmental chamber (THMS600, Linkam Scientific Instrument) and the humidity was controlled with a RH95 system (Linkam Scientific Instrument). For the in-situ Raman measurements (temperature and humidity), the excitation laser was probed through the spiro-OMeTAD layer of the device (note the measurements can be done through the glass

side of the pixel, however it takes significantly more time to be degraded). The probing conditions are: Raman mapping (3 mW, 0.5 s); PL mapping (0.03 mW, 0.01 s); in-situ Raman with temperature and humidity (0.6 mW, 30 s).

Fabrication of the perovskite PV module and the large area Raman mapping

The device structure of the perovskite PV module is glass/FTO/c-TiO_2/m-TiO_2/MAPI/m-ZrO_2/m-carbon, and it was encapsulated by glass. The module was fabricated in the following way: FTO on glass substrate was laser patterned to 5 pixels (size of substrate is 10 cm x 12 cm); c-TiO_2 by spray coating; m-TiO_2, m-ZrO_2 and m-carbon are screen-printed. PbI_2 solution was drop-cast on the active region through the meso-carbon, and the module was dipped in the MAI solution to convert to MAPI (active area ~ 10 cm x 1 cm for each pixel). Thicknesses of the layers are: ~50 nm for c-TiO_2; ~ 1 µm for m-TiO_2 and ZrO_2 and ~ 7 µm for m-carbon. The large area Raman mapping was performed by using the Wire 4.1 software with streamline mapping method with Slalom function (power: 6 mW; time: 0.1 s).

Acknowledgements

The authors would like to acknowledge funding from: Welsh Assembly Government funded Sêr Cymru Solar Project, Supergen Solar Challenge (EP/M025020/1), the M2A funding from the European Social Fund through the Welsh Government, Renishaw plc, Supersolar (EP/J017361/1), and the EPSRC Self-assembling Perovskite Absorbers - Cells Engineered into Modules (SPACE-Modules) EP/M015252/1. The authors would like to thank the EPSRC and TSB for supporting this work through the SPECIFIC Innovation and Knowledge Centre, and Linkam Scientific Instrument for lending us the humidity generator.

Notes and references

1 A. Kojima, K. Teshima, Y. Shirai and T. Miyasaka, *J. Am. Chem. Soc.,* 2009, **131**, 6050-6051.
2 H.-S. Kim, C.-R. Lee, J.-H. Im, K.-B. Lee, T. Moehl, A. Marchioro, S.-J. Moon, R. Humphry-Baker, J.-H. Yum, J. E. Moser, M. Grätzel and N-G. Park, *Sci. Rep.,* 2012, **2**, 591.
3 W. S. Yang, J. H. Noh, N. J. Jeon, Y. C. Kim, S. Ryu, J. Seo and S. I. Seok, *Science*, 2015, **348**, 1234-1237.
4 N. J. Jeon, J. H. Noh, W. S. Yang, Y. C. Kim, S. Ryu, J. Seo and S. I. Seok, *Nature,* 2015, **517**, 476-480.
5 G. Cotella, J. Baker, F. DeRossi, C. Pleydell-Pearce, M. Carnie and T. M. Watson, *Sol. Energ. Mat. Sol. Cells,* 2017, **159**, 362-369.
6 K. E. A. Hooper, B. Smith, P. Greenwood, J. Baker and T. M. Watson, *Mater. Res. Innov.* 2015, **7**, 482-487.
7 J. Yang, B. D. Siempelkamp, D. Liu and T. L. Kelly, *ACS Nano*, 2015, **9**, 1955-1963.
8 T. Leijtens, G. E. Eperon, S. Pathak, A. Abate, M. M. Lee and H. J. Snaith, *Nat. Commun.,* 2013, **4**, 2885.
9 D. Wang, M. Wright, N. K. Elumalai and A. Uddin, *Sol. Energ. Mat. Sol. Cells,* 2016, **147**, 255-275.
10 T. A. Berhe, W.-N. Su, C.-H. Chen, C.-J. Pan, J.-H. Cheng, H.-M. Chen, M.-C. Tsai, L.-Y. Chen, A. A. Dubaleb and B.-J. Hwang, *Energy Environ. Sci.,* 2016, **9**, 323-356.
11 J. Razzell-Hollis, J. Wade, W. C. Tsoi, Y. Soon, J. Durrant and J.-S. Kim, *J. Mater. Chem. A,* 2014, **2**, 20189-20195.
12 W. C. Tsoi, D. T. James, J. S. Kim, P. G. Nicholson, C. E. Murphy, D. D. C. Bradley, J. Nelson and J.-S. Kim, *J. Am. Chem. Soc.,* 2011, **133**, 9834-9843.
13 J. Yamamoto and Y. Furukawa, *Chem. Phys. Lett.,* 2016, **644**, 267-270.
14 C. Quarti, G. Grancini, E. Mosconi, P. Bruno, J. M. Ball, M. M. Lee, H. J. Snaith, A. Petrozza and F. De Angelis, *J. Phys. Chem. Lett.,* 2014, **5**, 279-284.
15 M. Ledinsky, P. Löper, B. Niesen, J. Holovský, S.-J. Moon, J.-H. Yum, S. De Wolf, A. Fejfar and Christophe Ballif, *J. Phys. Chem. Lett.,* 2015, **6**, 401-406.
16 B. W. Park, S. M. Jain, X. Zhang, A. Hagfeldt, G. Boschloo and T. Edvinsson, *ACS Nano,* 2015, **9**, 2088-2101.
17 J. Burschka, N. Pellet, S.-J. Moon, R. Humphry-Baker, P. Gao, M. K. Nazeeruddin and M. Grätzel, *Nature,* 2013, **499**, 316-319.
18 L. Zhang, T. Liu, L. Liu, M. Hu, Y. Yang, A. Mei and H. Han, J. *Mater. Chem. A*, 2015, **3**, 9165-9170.
19 A. Mei, X. Li, L. Liu, Z. Ku, T. Liu, Y. Rong, M. Xu, M. Hu, J. Chen, Y. Yang, M. Grätzel and H. Han, *Science*, 2014, **345**, 295-298.
20 R L McCreery, *Raman Spectroscopy for Chemical Analysis*, John Wiley & Sons Inc, New York, 2000.
21 E. Mosconi, A. Amat, M. K. Nazeeruddin, M. Graetzel and F. De Angelis, *J. Phys. Chem. C*, 2013, **117**, 13902-13913.
22 F. Tian, Y. Zhang, J. Zhang and C. J. Pan, *Phys. Chem. C,* 2012, **116**, 7515-7519.
23 N. Aristidou, I. Sanchez-Molina, T. Chotchuangchutchaval, M. Brown, L. Martinez, T. Rath and S. A. Haque, *Angew.Chem. Int. Ed.,* 2015, **54**, 8208-8212.
24 S. D. Stranks and H. J. Snaith, *Nature Nanotech.*, 2015, **10**, 391-402.
25 Z. Song, S. C. Watthage, A. B. Phillips, G. K. Liyanage, R. R. Khanal, B. L. Tompkins, R. J. Ellingson and M. J. Heben, *Proc. SPIE*, 2015, 9561.
26 B. Philippe, B.-W. Park, R. Lindblad, J. Oscarsson, S. Ahmadi, E. M. J. Johansson and Håkan Rensmo, *Chem. Mater.,* 2015, **27**, 1720-1731.
27 A. M. A. Leguy, Y. Hu, M. Campoy-Quiles, M. I. Alonso, O. J. Weber, P. Azarhoosh, M. van Schilfgaarde, M. T. Weller, T. Bein, J. Nelson, P. Docampo and P. R. F. Barnes, *Chem. Mater.,* 2015, **27**, 3397-3407.
28 J. A. Christians, P. A. M. Herrera and P. V. Kamat, *J. Am. Chem. Soc.,* 2015, **137**, 1530-1538.
29 Y. Wu, A. Islam, X. Yang, C. Qin, J. Liu, K. Zhang, W. Penga and L. Han, *Energy Environ. Sci.*, 2014, **7**, 2934-2938.
30 R.D. Deegan, O. Bakajin, T. F. Dupont, G. Huber, S. R. Nagel and T. A. Witten, *Nature*, 1997, **389** , 827-829.

